JOURNAL OF AIRCRAFT
Vol. 32, No. 3, May–June 1995

Computation of Delta-Wing Roll Maneuvers

Raymond E. Gordnier*
U.S. Air Force Wright Laboratory, Wright-Patterson Air Force Base, Ohio 45433

This article presents computations of delta-wing roll maneuvers for an 80-deg sweep delta-wing at 30-deg angle of attack. Three constant roll-rate maneuvers are considered. Two of the maneuvers consist of a roll from 0 to 45 deg at nondimensional roll rates of Φ = 0.0233 and 0.0467. The third roll maneuver computed starts at a 45-deg roll angle and rolls back to a −45-deg roll angle at a roll rate Φ = −0.0467. The governing equations are the unsteady, three-dimensional Navier–Stokes equations. The equations are solved using the implicit, approximately-factored, diagonal form of the Beam–Warming algorithm. Subiterations are used to provide a more accurate means of implementing the diagonal form of the algorithm for unsteady flows. The effects of roll-rate and differing initial roll angles on the dynamical behavior of the vortices positions and strengths as well as their corresponding effect on surface pressure and roll moment coefficient are described.

Nomenclature

a_b = body acceleration
Cl = roll moment coefficient
C_p = pressure coefficient
C_{p_0} = total pressure coefficient
E_t = total energy
J = transformation Jacobian
L = reference length, root chord
M_∞ = freestream Mach number
Pr = Prandtl number
p = pressure
Re = Reynolds number
S = local semispan
s = halfspan
T = temperature
t = nondimensional time $\bar{t}u_\infty/L$
u, v, w = velocity components in x, y, and z
X, Y, Z = body-fixed coordinates
x, y, z = physical coordinates
α = angle of attack
Λ = sweep angle
μ = viscosity coefficient
ξ, η, ζ = computational coordinates
ρ = density
τ_{ij} = stress tensor
Φ = nondimensional roll rate, $\dot{\phi}s/u_\infty$
ϕ = roll angle
$\dot{\phi}$ = roll rate, rad/s
ω = angular velocity

Introduction

IN designing a modern fighter aircraft a number of competing attributes influence its combat effectiveness. Two important contributing factors are the aircraft's maneuverability and agility. In a recent paper by Skow,[1] discussing the importance of agility in contributing to a balanced design for a fighter, he states that torsional (or roll) agility ranked first in order of agility payoff, followed by axial and pitch agility. Skow defines agility as the ability of the fighter to minimize time delays between target acquisition and target destruction. It is therefore important to understand the aerodynamics of transient, high roll-rate maneuvers.

The majority of effort in understanding roll-type maneuvers in recent years has focused on the study of self-sustained delta-wing rock observed for high sweep delta-wings at moderate to large angles of attack. A number of recent experiments have investigated the delta-wing roll dynamics through free and forced oscillations.[2–10] These investigations have been carried out in both water and wind tunnels and have predominantly focused on flow visualization and force and moment measurements. Unsteady surface pressure measurements have also been reported by Hanff and Jenkins[6] and Arena.[5] These experiments have highlighted several important contributing factors to delta-wing rock including: an instability at small roll angles and damping lobes at larger roll angles for the roll-moment coefficient,[2,4,9] the importance of vortex position and strength during wing-rock in creating the instability to drive wing-rock motion,[2,7,9] and the roll response to roll angle and roll rate, subject to convective time lag effects.[7,8,10] In addition, when vortex breakdown occurs, its dynamic effect is influenced by roll-rate-induced conical camber.[8,10]

A number of numerical investigations of wings undergoing forced rolling motions have been reported. The majority of these computations for forced roll oscillations have assumed either conical[11–14] or inviscid[15] flow, limiting their fidelity to the flow physics. Chaderjian[16] has presented computations for a forced rocking motion using the three-dimensional, thin-layer Navier-Stokes equations. Kandil and Salman[15] and Lee and Batina[14] have coupled their computations with the equations of motion to actually consider true wing-rock.

The focus of this work will be on the numerical simulation of a constant roll-rate maneuver from an initial roll angle ϕ_i to a final roll angle ϕ_f. This type of roll maneuver is performed routinely by a fighter aircraft and a better understanding of its aerodynamics will aid in designing a more maneuverable and agile aircraft. Computations of a constant roll-rate Φ = 0.0233 maneuver from 0 to 45 deg were first reported by the author in Ref. 17. In the present study the effects of increasing the roll rate and starting at a different (nonzero) roll angle are investigated. Two additional roll maneuvers are computed, one from 0 to 45 deg at double the first roll rate Φ = 0.0467, and the second starting at an initial roll angle ϕ_i = 45 deg and rolling to a final roll angle ϕ_f = −45 deg, at a roll rate Φ = −0.0467.

Governing Equations

The governing equations for the present problem are the unsteady, three-dimensional Navier–Stokes equations writ-

Presented as Paper 93-2975 at the AIAA 24th Fluid Dynamics Conference, Orlando, FL, July 6–9, 1993; received Feb. 1, 1994; revision received Aug. 22, 1994; accepted for publication Aug. 26, 1994.

*Aerospace Engineer, CFD Research Branch, Aeromechanics Division. Senior Member AIAA.

ten in strong conservation form,[18] using a general, time-dependent coordinate transformation ξ, η, ζ, t:

$$\frac{\partial}{\partial t}\left(\frac{q}{J}\right) + \frac{\partial \hat{F}}{\partial \xi} + \frac{\partial \hat{G}}{\partial \eta} + \frac{\partial \hat{H}}{\partial \zeta} = \frac{1}{Re}\left(\frac{\partial \hat{F}_v}{\partial \xi} + \frac{\partial \hat{G}_v}{\partial \eta} + \frac{\partial \hat{H}_v}{\partial \zeta}\right) \quad (1)$$

where

$$q = \begin{bmatrix} \rho \\ \rho u \\ \rho v \\ \rho w \\ \rho E_t \end{bmatrix}, \qquad \hat{F} = \frac{1}{J}\begin{bmatrix} \rho U \\ \rho u U + \xi_x p \\ \rho v U + \xi_y p \\ \rho w U + \xi_z p \\ \rho E_t U + p\tilde{U} \end{bmatrix}$$

$$\hat{G} = \frac{1}{J}\begin{bmatrix} \rho V \\ \rho u V + \eta_x p \\ \rho v V + \eta_y p \\ \rho w V + \eta_z p \\ \rho E_t V + p\tilde{V} \end{bmatrix}, \qquad \hat{H} = \frac{1}{J}\begin{bmatrix} \rho W \\ \rho u W + \zeta_x p \\ \rho v W + \zeta_y p \\ \rho w W + \zeta_z p \\ \rho E_t W + p\tilde{W} \end{bmatrix}$$

$$\hat{F}_v = \frac{1}{J}\begin{bmatrix} 0 \\ \xi_{x_i}\tau_{i1} \\ \xi_{x_i}\tau_{i2} \\ \xi_{x_i}\tau_{i3} \\ \xi_{x_i}b_i \end{bmatrix}, \qquad \hat{G}_v = \frac{1}{J}\begin{bmatrix} 0 \\ \eta_{x_i}\tau_{i1} \\ \eta_{x_i}\tau_{i2} \\ \eta_{x_i}\tau_{i3} \\ \eta_{x_i}b_i \end{bmatrix}, \qquad \hat{H}_v = \frac{1}{J}\begin{bmatrix} 0 \\ \zeta_{x_i}\tau_{i1} \\ \zeta_{x_i}\tau_{i2} \\ \zeta_{x_i}\tau_{i3} \\ \xi_{x_i}b_i \end{bmatrix}$$

$$U = \xi_t + \xi_x u + \xi_y v + \xi_z w = \xi_t + \tilde{U}$$

$$V = \eta_t + \eta_x u + \eta_y v + \eta_z w = \eta_t + \tilde{V}$$

$$W = \zeta_t + \zeta_x u + \zeta_y v + \zeta_z w = \zeta_t + \tilde{W}$$

$$E_t = e + \tfrac{1}{2}(u^2 + v^2 + w^2)$$

$$b_i = u_j\tau_{ij} + \frac{\mu}{(\gamma - 1)PrM_\infty^2}\frac{\partial \xi_l}{\partial x_i}\frac{\partial T}{\partial \xi_l}$$

$$\tau_{ij} = \mu\left(\frac{\partial \xi_k}{\partial x_j}\frac{\partial u_i}{\partial \xi_k} + \frac{\partial \xi_k}{\partial x_i}\frac{\partial u_j}{\partial \xi_k}\right) - \frac{2}{3}\mu\delta_{ij}\frac{\partial \xi_l}{\partial x_k}\frac{\partial u_k}{\partial \xi_l}$$

$$x_1, x_2, x_3 \rightarrow x, y, z$$

$$\xi_1, \xi_2, \xi_3 \rightarrow \xi, \eta, \zeta$$

The system of equations is closed using the perfect gas law, Sutherland's formula for viscosity, and the assumption of a constant Prandtl number $Pr = 0.72$. Flow quantities have been nondimensionalized by their respective freestream values, except for pressure, which is nondimensionalized by twice the freestream dynamic pressure, and speed of sound, which is nondimensionalized by the freestream velocity. All lengths have been normalized by the root chord length of the delta-wing.

Numerical Procedure

The governing equations are solved numerically using the implicit, approximately-factored algorithm of Beam and Warming.[19] The equations are discretized using Euler implicit time-differencing and second-order accurate central differences for all spatial derivatives. A blend of second- and fourth-order nonlinear dissipation, as suggested by Jameson,[20] is used to stabilize the central difference scheme. The current work, in which subsonic flows are investigated, requires only fourth-order dissipation. In the present numerical scheme both a full block tridiagonal inversion scheme and a diagonalized inversion scheme based on the diagonal form of the Beam–Warming algorithm developed by Pulliam and Chaussee[21] are available.

A subiteration procedure that has been successfully used by several authors[22–24] has also been incorporated as an option in the current solution procedure.[25] The subiteration strategy provides distinct improvements to the numerical scheme. The stability limits of the three-factored algorithm are relaxed by reducing the factorization error through subiterations. This greatly improves the efficiency of the algorithm. Subiterations also provide improved time accuracy when implementing the diagonal form of the Beam–Warming algorithm for unsteady flows.

A fully vectorized, time-accurate code has been developed to implement the aforementioned scheme.[26] The computational requirements are 33 words/grid-point and a processing rate of 1.8×10^{-5} CPU s/grid-point/iteration for the diagonal solver on a Cray II. The block tridiagonal solver processing rate is approximately twice that of the diagonal solver. The code has been validated for a variety of steady and unsteady flows. Both supersonic and subsonic flows over delta-wings, including vortex breakdown[17,25,27–29] have been computed with this code. Unsteady flow simulations have been carried out for both a pitching slender body of revolution[30] and pitching and rolling delta-wings.[17,29] Finally, the code has been used to calculate steady and unsteady horseshoe vortex flows around a cylinder/flat plate juncture.[26,31] These results have provided a broad validation base for both steady and unsteady flows.

For the body motion to be considered in this study (i.e., delta-wing roll), a general time-dependent coordinate transformation is introduced. The rigid, nondeforming grid is allowed to roll with the body, and the grid motion is treated through the general coordinate transformation. This approach eliminates the need for generating multiple grids. Also, since the equations are written in an inertial frame of reference, no additional terms are required in the governing equations with the effects of motion appearing in the boundary conditions.

Grid Structure and Boundary Conditions

The delta-wing configuration used for the present computations corresponds to the delta-wing model used by Arena[9] in his experimental wing-rock studies. The wing has an 80-deg leading-edge sweep, a root chord of $16\frac{5}{8}$ in., a thickness of $\frac{1}{4}$ in., and a 45-deg bottom side bevel at the leading edge. In the computational configuration the trailing edge has also been beveled (9.3 deg) to provide for a smooth closure of the grid for the wing.

The grid chosen for the current study has an H-O structure, with O-grids being stacked axially along the delta-wing. This grid topology provides good resolution of the leading-edge vortices and the apex region of the delta-wing. The baseline grid used for these computations consists of 219 points around the body, 81 points normal to the body with a minimum spacing at the wall of $\Delta z = 0.0001$, and 89 points in the axial direction with a constant grid spacing of $\Delta x = 0.025$ over the predominant portion of the wing. The computational domain extends 1 chord upstream of the wing, 1.5 chords downstream of the wing, and 1.5 chords in the normal direction from the wing.

The boundary conditions for the delta-wing roll problem are implemented as follows. Characteristic boundary conditions are applied at the far-field and upstream boundaries. At the downstream boundary first-order extrapolation of the interior flow values is used. On the delta-wing surface the following conditions are applied:

$$\boldsymbol{u} = \boldsymbol{u}_b$$

$$\frac{\partial T}{\partial \eta} = 0$$

$$\frac{\partial p}{\partial n} = -\rho \boldsymbol{a}_b \cdot \boldsymbol{n}$$

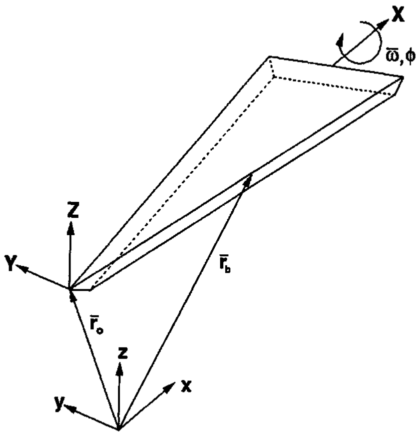

Fig. 1 Problem layout.

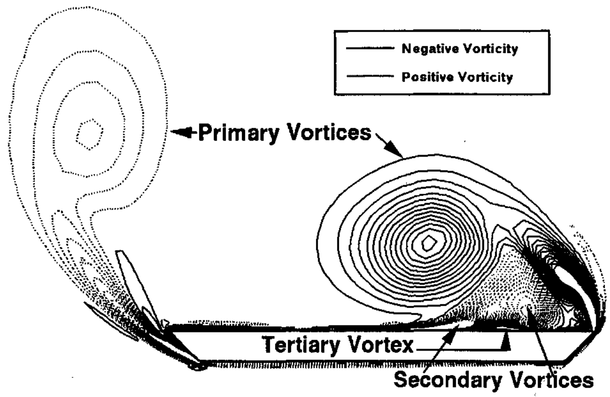

Fig. 2 Contours of the axial component of vorticity: $X/L = 0.6$, $\phi = 45$ deg.

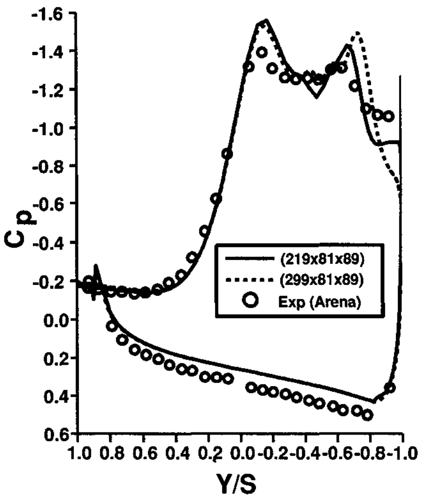

Fig. 3 Surface pressure coefficient: $X/L = 0.6$, $\phi = 45$ deg.

where u_b and a_b are the velocity and acceleration of the point on the body defined as

$$u_b = \omega \times (r_b - r_0)$$

$$a_b = \frac{d\omega}{dt} \times (r_b - r_0) + \omega \times [\omega \times (r_b - r_0)]$$

and n is the surface normal vector (see Fig. 1). For the case of roll about a fixed axis considered here, $r_0 = 0$ and $\omega = \Phi \mathbf{i}$, where Φ is the nondimensional roll rate.

For the H-O grid structure adopted for the present problem, a singular line emanates from the apex of the delta-wing. Additionally, a singular plane bounded by two singular lines is located downstream of the trailing edge. These singular surfaces are the continuation of the grid from the wing surface upstream and downstream of the delta-wing. The flow variables on these surfaces are obtained by extrapolating the conserved variables to the surface and then performing the appropriate averaging.

Results—Static

Experimental data obtained by Arena[9] for this delta-wing at fixed roll angles has been used to demonstrate the capabilities of the present numerical scheme. The flow conditions for the experiment were Reynolds number $Re = 4 \times 10^5$, angle of attack $\alpha = 30$ deg, and nominally incompressible flow. For the computations, similar conditions are considered with the exception of freestream Mach number, which is set to $M_\infty = 0.2$. The results discussed are typical of a more extensive comparison reported in Ref. 17.

The computed results presented are for a fixed roll angle $\phi = 45$ deg. Figure 2 shows the vortex structure for this case at a typical cross plane $X/L = 0.6$. The right vortex (downward leading edge) has moved inboard and towards the surface of the wing creating an extensive secondary flow region. The left vortex (upward leading edge) has moved outboard of the wing and away from the surface. Its influence on the flow over the upper surface of the delta-wing is greatly diminished. The shear layer that rolls up to form this vortex now emanates from the lower surface bevel rather than the upward leading edge.

Figure 3 compares the computed surface pressure at $X/L = 0.6$ with the experimental measurements of Arena.[9] Solutions for both the baseline grid and a refined grid are shown. The refined grid has the same axial distribution of grid points, 40 additional grid points across the span of the wing, and the grid distribution in the body normal direction has been modified to provide enhanced resolution in the region of the vortex cores while maintaining the same number of grid points. Both computed solutions agree well with the experimental measurements, with only a slight overexpansion in the region under the right vortex. Slight differences in the solution in this region are seen for the refined grid. Elsewhere the two solutions are virtually identical. This figure also reflects the reduction in influence of the left vortex on the surface pressure with the expansion peak due to the left vortex being eliminated.

Results—Dynamic

The roll maneuvers computed are of constant roll rate Φ, from an initial roll angle ϕ_i, to a final roll angle ϕ_f. For each maneuver a smooth acceleration to and deceleration from the constant roll rate occurs over the dimensionless time period $\Delta t = 0.25$. Table 1 gives these parameter values for each of the cases considered. The roll rate $\Phi = 0.0233$ corresponds to the mean roll rate for one cycle in the wing-rock experiments of Arena.[9] Since no experimental data exists for this maneuver, the computations are run at a low Reynolds number $Re = 1.0 \times 10^4$. This eliminates questions related to turbulence, transition, or the susceptibility to and effect of shear-layer instabilities.[32] Furthermore, computing at low Reynolds numbers provides improved grid resolution for the same number of grid points. These low Reynolds number computations are expected to produce similar qualitative behavior to higher Reynolds number cases for the vortex dynamics due to rolling motion considered here. The time step used for the unsteady computation is $\Delta t = 0.001$.

The computation of these roll maneuvers for a delta-wing is very costly, requiring approximately 225 CPU h on a Cray II for case I. In order to minimize the computing time required, the diagonal form of the algorithm is used with two subiterations. The subiterations reduce the effect of the tem-

Table 1 Roll maneuver parameters

Case	ϕ_i	ϕ_f	Φ
I	0	45	0.0233
II	0	45	0.0467
III	45	−45	−0.0467

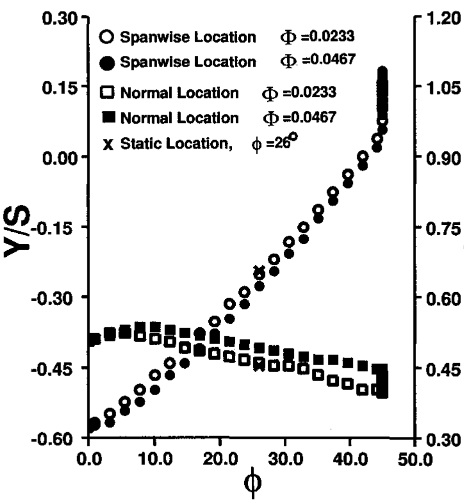

Fig. 4 Right (downward rolling edge) vortex core location at X/L = 0.9 for two roll rates.

poral errors introduced in the diagonalization process. This technique for computing unsteady flowfields in forced motion has been compared with the use of a fully time accurate block tridiagonal solver for the problem of two-dimensional dynamic stall. A comparison (not included) up to and through the formation of the dynamic stall vortex showed virtually no difference in the two solutions.

Different Roll Rates

The effect of increasing the roll rate is studied by comparing results for cases I and II. In a previous work[17] an extensive discussion of case I was presented. The overall dynamic behavior of the vortices at $X/L = 0.9$ was described as follows. As the wing rolls, the right vortex (downward leading edge) moves inboard on the wing and towards the surface. The left vortex moves outboard of the wing and away from the surface. As the right vortex moves inboard and towards the surface the associated secondary flow grows in size and influence. As the left vortex moves outboard and away from the surface the secondary flow associated with this vortex decreases and eventually disappears.

Figures 4 and 5 compare the locations of the vortex cores for cases I and II at $X/L = 0.9$. The vortex core location is defined as the point of minimum total pressure. These figures show that the right (downward rolling edge) vortex moves inboard and towards the surface, and the left vortex (upward rolling edge) shifts outboard and away from the surface. In the spanwise direction increasing the roll rate delays the motion of the vortex cores for both vortices. This leads to a lagging of approximately 2 deg of roll in the spanwise location of the vortex cores between the higher and lower roll rates. The spanwise vortex position is also seen to lag after the wing stops with the right and left vortices moving by an additional $\Delta Y/S = 0.11$ and $\Delta Y/S = 0.082$, for the higher roll rate, respectively.

For the left vortex (Fig. 5), the body normal position of the core initially moves towards the surface before moving away from the surface. The roll angle at which the vortex core passes through the same normal location differs typically by approximately 10 deg between the lower and higher roll rate. Increasing the roll rate causes the vortex core to move closer to the surface before moving away from the surface. A significant motion of the core away from the surface occurs after the wing stops, with the core moving by $\Delta Z/S = 0.13$ for the higher roll rate. The body normal position of the right vortex core initially moves away from the surface before moving towards the surface. Increasing the roll rate causes the vortex core to move slightly further away from the body before moving towards the surface. The effect is not as great as that seen for the upward rolling-edge vortex, however. As the final roll angle of 45 deg is approached and the wing stops, the right vortex is closer to the surface and moves away for the low roll rate, whereas it is further away and moves towards the surface for the higher roll rate. This difference is attributable mainly to the dynamic behavior of the secondary flow (observed in an animation not presented here). The body normal motion after the wing stops is significantly larger for the left vortex than for the right vortex.

An indication of the vortex strength is obtained by examining the minimum total pressure in the vortex core. Figure 6 compares the variation of the minimum pressure in the vortex cores during the roll maneuver for the two roll rates. The right vortex initially shows a small decrease in the total pressure at the core before it increases for higher roll angles. The principal effect of increasing the roll rate is to shift the roll angle where the increase in total pressure begins by ap-

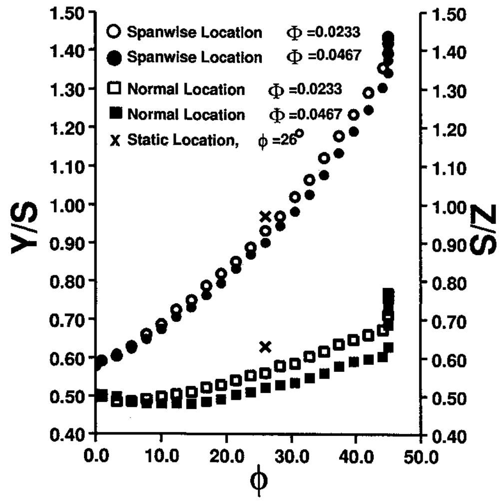

Fig. 5 Left (upward rolling edge) vortex core location at X/L = 0.9 for two roll rates.

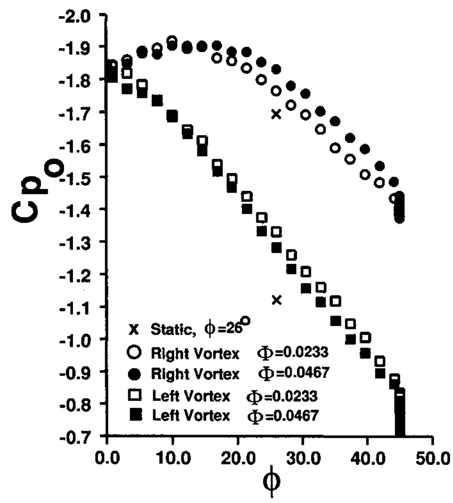

Fig. 6 Minimum total pressure coefficient in vortex core during roll at X/L = 0.9 for two roll rates.

proximately 4.5 deg. The rate of increase of the total pressure after this point is nearly the same for each roll rate. The core of the left vortex shows a continual gain in total pressure during the roll maneuver. Increasing the roll rate has minimal effect on the minimum total pressure during the maneuver. Both vortices show a significant difference between the total pressure when the wing stops and the final value attained.

Figure 7 compares the roll moment coefficient for the two roll rates. The roll moment shows an initial sharp increase due to the acceleration of the wing. It then decreases until a local minimum is attained, after which point it again increases until there is a rapid decrease in the roll moment associated with stopping the roll motion. The primary effect of the change in roll rate is seen where the wing accelerates and decelerates. Since the wing was allowed to achieve its final constant roll rate over the same amount of time for each case, the case with higher roll rate will have a larger acceleration and deceleration and a correspondingly larger increase and decrease in the roll moment. The angle for the minimum value of roll moment is shifted by 2 deg from $\phi = 31.5$ deg for the low roll rate to $\phi = 33.5$ deg for the high roll rate.

The behavior of the roll moment coefficient can be further understood by considering the vortex position and strength and their effect on the surface pressure of the wing. In Fig. 5, for the higher roll rate, the left vortex is closer to the wing surface and more inboard than the lower roll-rate case. This leads to the more extensive low-pressure region near the upward moving leading edge for the higher roll rate. Similarly, the right vortex is closer to the wing surface and further inboard for the lower roll rate, leading to a more extensive lower pressure region on the right-half of the wing. These surface pressure effects combined with the acceleration effects lead to the larger restoring moment for the lower roll rate case. The shift in location of the minimum roll moment is due to the small lag in the spanwise position of the vortices, which delays the influence of the right vortex on the left half of the wing thus shifting the minimum in roll moment.[17]

Different Initial Roll Angle

Case III considers a roll maneuver that starts from a nonzero initial roll angle. This case starts from the end of the hold portion of case II and rolls back through 0-deg to a −45-deg roll angle. Comparing these two cases allows study of the effect of starting the roll maneuver with a nonzero initial roll angle. Figures 10–12 show a combination of case II and case III.

Figures 8 and 9 show the motion of the right and left vortex cores, respectively, at an axial location $X/L = 0.9$. Hysteresis in both the spanwise and body normal locations of both vortex cores is observed. The body normal position of the left vortex displays the largest hysteresis with $\Delta Z/S = 0.315$ at a roll angle $\phi = 35.1$ deg. The right vortex shows significantly less hysteresis in the body normal position of the core with a maximum difference of $\Delta Z/S = 0.12$ at a roll angle $\phi = 12.3$ deg. The large hysteresis loop observed in the normal position of the left vortex is due to the lag in the body normal motion of the vortex associated with the upward moving leading edge. The spanwise position of the vortex cores also shows a hysteresis effect. The right vortex locus has a slightly larger maximum difference $\Delta Y/S = 0.227$ as opposed to $\Delta Y/S = 0.17$ for the left vortex. This difference in the spanwise motion of the right vortex is due in part to the influence of the large secondary flow that develops.

Figure 10 displays the variation of the strength of the right and left vortices as indicated by the minimum total pressure in the vortex core. A sizable hysteresis is seen in the strength of the right vortex. The vortex is stronger when the right half of the wing rolls down and the vortex moves inboard and towards the surface than when the wing rolls back and the vortex moves outboard and away from the surface. Only a small hysteresis at higher roll angles is seen for the left vortex.

The roll moment coefficient for cases II and III is plotted in Fig. 11. The significant effect of the initial acceleration and the final deceleration is again clearly evident. This effect is partly responsible for the much larger restoring moment when

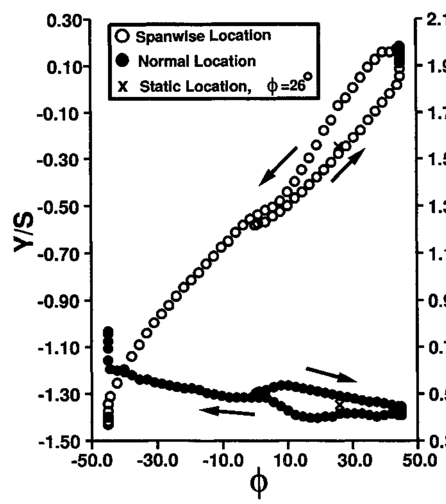

Fig. 8 Comparison of the right vortex core location at $X/L = 0.9$ for cases II and III.

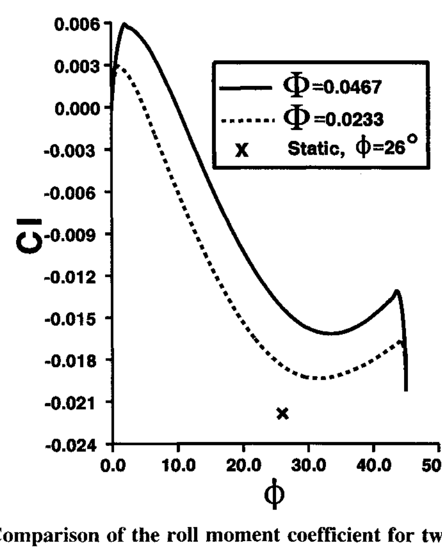

Fig. 7 Comparison of the roll moment coefficient for two roll rates.

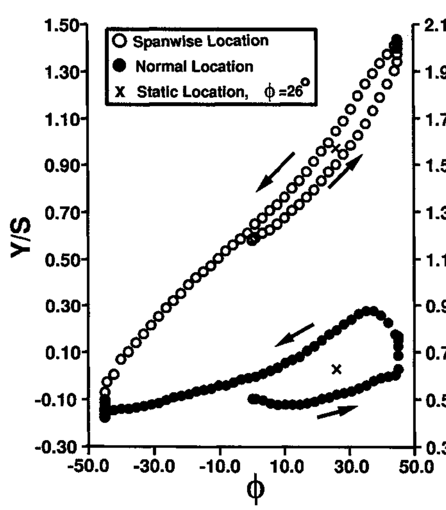

Fig. 9 Comparison of the left vortex core location at $X/L = 0.9$ for cases II and III.

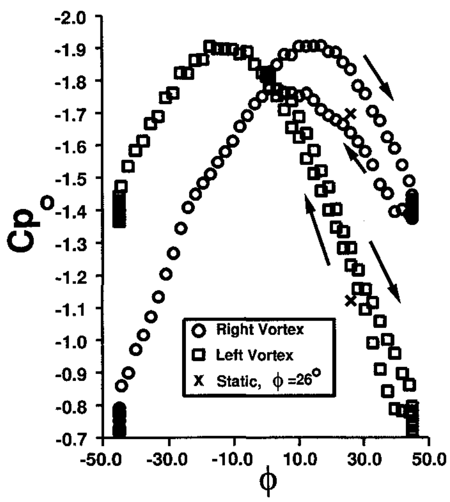

Fig. 10 Minimum total pressure coefficient in vortex core during roll at X/L = 0.9 for cases II and III.

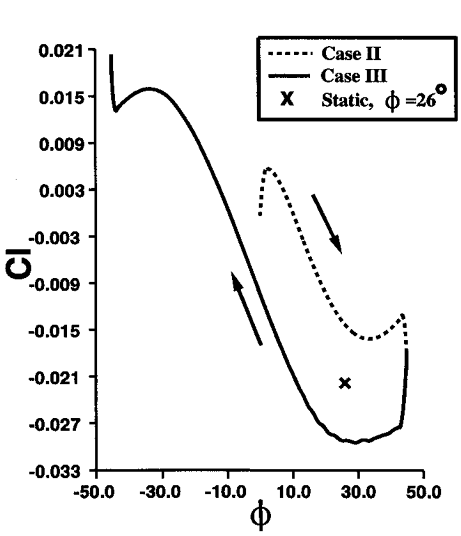

Fig. 11 Roll moment coefficient for cases II and III.

the wing rolls back in case III. A difference in the qualitative behavior between when the wing rolls from 0 to 45 deg (forward), and when the wing rolls from 45 deg back towards 0 deg (backwards) is also noted. As the wing rolls backward, the roll moment coefficient attains a minimum at a roll angle ϕ = 29.1 deg, as opposed to ϕ = 33.5 deg when the wing is rolling forward. The curve around the minimum when the wing rolls backwards is also broader and shallower than when the wing rolls forward. The hysteresis in the position of the left vortex appears to be the main contributing factor to this difference since it delays the development of a larger positive roll moment from the left half of the wing due to the suction created by the left vortex. As the wing rolls back towards a −45-deg roll angle, a local maximum of Cl = 0.016 is achieved at a roll angle of ϕ = −33.8 deg, which corresponds with the appropriate antisymmetric values of ϕ = 33.5 deg and Cl = −0.016 during the forward rolling portion of the maneuver. Therefore, any influence of the initial condition on the roll moment has been largely overcome at this time in the maneuver.

The hysteresis in vortex position and strength also influences the surface pressure. Figure 8 showed that the right vortex core is located slightly outboard and further away from the wing as the wing rolls forward, and is inboard and closer to the wing as the wing rolls back. The right vortex is much stronger, however, as the wing rolls forward than when the wing rolls back (Fig. 10). This leads to a low-pressure region under the right vortex that is stronger and more extensive than the static case as the wing rolls forward, and is slightly weaker and less extensive as the wing rolls back. Figure 9 showed that there is a significant hysteresis in the body normal position of the left vortex, with the vortex core being closer to the wing as the wing rolls forward, and further away as the wing rolls back. Also, the left vortex is more inboard on the wing as the wing rolls forward than when the wing is rolling back. No significant hysteresis in the strength of the left vortex is observed (Fig. 10). Therefore, the low-pressure region due to the left vortex is stronger and extends further downstream as the wing rolls forward, and is weaker and does not extend as far downstream when the wing rolls back. This difference in pressure occurs near the leading edge where it has greater influence on the roll moment. Therefore, the hysteresis in the position of the left vortex is also an important contributing factor to the difference in the roll moment between cases II and III.

Summary

Three separate constant roll-rate maneuvers have been computed for an 80-deg sweep delta-wing at 30-deg angle of attack. Two of the maneuvers consist of a roll from 0 to 45 deg at nondimensional roll rates of Φ = 0.0233 and 0.0467, whereas the third maneuver considered starts at a roll angle of 45 deg and rolls to a −45-deg roll angle with a roll rate Φ = −0.0467. The unsteady, three-dimensional, full Navier-Stokes equations are solved using the diagonal form of the approximately-factored, Beam-Warming algorithm with subiterations.

For the same maneuver, increasing the roll rate tends to increase the lag observed in the motion of the vortex cores. The most significant effect is seen in the body normal position of the upward-moving edge vortex. Only a minimal difference in the strength of the upward-moving edge vortex is seen. The roll angle where the strength of the downward-moving-edge vortex begins to decrease is shifted by approximately 4.5 deg in roll. The effect of these differences in the motion and strength of the vortices on the surface pressure and the effect of the initial acceleration lead to larger restoring moments for the lower roll rate.

When comparing the roll maneuver for case II with case III, hysteresis in both the spanwise and body normal locations of the vortex cores is observed. The largest effect is again seen in the left (initially upward moving edge) vortex due to the lag in the body normal position of the vortex. Significant hysteresis in vortex strength is only seen in the right vortex. The vortex is stronger as the wing rolls down and weaker as the wing rolls upward. The hysteresis in the roll moment coefficient is attributable both to the effects of acceleration and deceleration and the effect of the hysteresis in the position of the left vortex on the surface pressure.

Acknowledgments

Computational resources were provided by NASA Ames Research Center, Moffett Field, California, under the NAS Program, and by the Phillips Laboratory Supercomputer Center, Kirtland Air Force Base, New Mexico. The author wishes to thank Andrew Arena for providing the experimental results for validation. Miguel Visbal provided many valuable insights and discussions during the preparation of this work.

References

[1]Skow, A. M., "Agility as a Contributor to Design Balance," *Journal of Aircraft*, Vol. 29, No. 1, 1992, pp. 34–46.

[2]Nguyen, L. T., Yip, L., and Chambers, J. R., "Self-Induced Wing Rock of Slender Delta Wings," AIAA Paper 81-1883, Aug. 1981.

[3]Levin, D., and Katz, J., "Dynamic Load Measurements with Delta Wings Undergoing Self-Induced Roll-Oscillations," *Journal of Aircraft*, Vol. 21, No. 1, 1984, pp. 30–36.

[4]Morris, S. L., and Ward, D. T., "A Video-Based Experimental Investigation of Wing Rock," *AIAA Atmospheric Flight Mechanics Conference*, AIAA, Washington, DC, 1989, pp. 25–35 (AIAA Paper 89-3349).

[5]Arena, A. S., "An Experimental Study of the Nonlinear Wing Rock Phenomenon," M.S. Thesis, Univ. of Notre Dame, Notre Dame, IN, April 1990.

[6]Hanff, E. S., and Jenkins, S. B., "Large-Amplitude High-Rate Roll Experiments on a Delta and Double Delta Wing," AIAA Paper 90-0224, Jan. 1990.

[7]Ng, T. T., Malcolm, G. N., and Lewis, L. C., "Experimental Study of Vortex Flows over Delta Wings in Wing-Rock Motion," *Journal of Aircraft*, Vol. 29, No. 4, 1992, pp. 598–603.

[8]Ericsson, L. E., and Hanff, E. S., "Unique High-Alpha Roll Dynamics of a 65 Deg Delta Wing," AIAA Paper 92-0276, Jan. 1992.

[9]Arena, A. S., "An Experimental and Computational Investigation of Slender Wings Undergoing Wing Rock," Ph.D. Dissertation, Univ. of Notre Dame, IN, April 1992.

[10]Ericsson, L. E., and Hanff, E. S., "Further Analysis of High-Rate Rolling Experiments of a 65 Deg Delta Wing," AIAA Paper 93-0620, Jan. 1993.

[11]Kandil, O. A., and Chuang, H. A., "Computation of Steady and Unsteady Vortex-Dominated Flows with Shock Waves," *AIAA Journal*, Vol. 26, No. 5, 1988, pp. 524–531.

[12]Kandil, O. A., and Chuang, H. A., "Unsteady Delta-Wing Flow Computation Using an Implicit Factored Euler Scheme," *AIAA Journal*, Vol. 28, No. 9, 1990, pp. 1589–1595.

[13]Batina, J. T., "Vortex-Dominated Conical-Flow Computations Using Unstructured Adaptively-Refined Meshes," AIAA Paper 89-1816, June 1989.

[14]Lee, E. M., and Batina, J. T., "Conical Euler Simulation and Active Suppression of Delta Wing Rocking Motion," NASA TM 102683, Oct. 1990.

[15]Kandil, O. A., and Salman, A. A., "Three-Dimensional Simulation of Slender Delta Wing Rock and Divergence," AIAA Paper 92-0280, Jan. 1992.

[16]Chaderjian, N. M., "Navier-Stokes Prediction of Large-Amplitude Delta-Wing Roll Oscillations Characterizing Wing Rock," *AIAA Atmospheric Flight Mechanics Conference*, AIAA, Waashington, DC, 1992, pp. 265–279 (AIAA Paper 92-4428).

[17]Gordnier, R. E., and Visbal, M. R., "Numerical Simulation of Delta-Wing Roll," AIAA Paper 93-0554, Jan. 1993.

[18]Pulliam, T. H., and Steger, J. L., "Implicit Finite-Difference Simulation of Three-Dimensional Compressible Flows," *AIAA Journal*, Vol. 18, No. 2, 1980, pp. 159–167.

[19]Beam, R. M., and Warming, R. F., "An Implicit Factored Scheme for the Compressible Navier-Stokes Equations," *AIAA Journal*, Vol. 16, No. 4, 1978, pp. 393–402.

[20]Jameson, A., Schmidt, W., and Turkel, E., "Numerical Solutions of the Euler Equations by Finite Volume Methods Using Runge-Kutta Time-Stepping Schemes," AIAA Paper 81-1259, June 1981.

[21]Pulliam, T. H., and Chaussee, D. S., "A Diagonal Form of an Implicit Approximate-Factorization Algorithm," *Journal of Computational Physics*, Vol. 39, No. 2, 1981, pp. 347–363.

[22]Rai, M. M., and Chakravarthy, S. R., "An Implicit Form for the Osher Upwind Scheme," *AIAA Journal*, Vol. 24, No. 5, 1986, pp. 735–743.

[23]Simpson, L. B., and Whitfield, D. L., "A Flux-Difference Split Algorithm for Unsteady Thin-Layer Navier-Stokes Solutions," *AIAA 9th Computational Fluid Dynamics Conference*, AIAA, Washington, DC, 1989, pp. 634–642 (AIAA Paper 89-1995).

[24]Taylor, A. C., III, Ng, W.-F., and Walters, R. W., "Upwind Relaxation Methods for the Navier-Stokes Equations Using Inner Iterations," *AIAA 9th Computational Fluid Dynamics Conference*, AIAA, Washington, DC, 1989, pp. 261–269 (AIAA Paper 89-1954).

[25]Gordnier, R. E., and Visbal, M. R., "Numerical Simulation of the Unsteady Vortex Structure over a Delta Wing," AIAA Paper 91-1811, June 1991.

[26]Visbal, M. R., "Numerical Investigation of Laminar Juncture Flows," AIAA Paper 89-1873, June 1989.

[27]Webster, W. P., and Shang, J. S., "Thin-Layer Full Navier-Stokes Simulations over a Supersonic Delta Wing," *AIAA Journal*, Vol. 29, No. 9, 1991, pp. 1363–1369.

[28]Webster, W. P., and Shang, J. S., "Numerical Simulation of Vortex Breakdown over a Subsonic Delta Wing," AIAA Paper 91-1814, June 1991.

[29]Visbal, M. R., "Structure of Vortex Breakdown on a Pitching Delta Wing," AIAA Paper 93-0434, Jan. 1993.

[30]Stanek, M. J., and Visbal, M. R., "Investigation of Vortex Development on a Pitching Slender Body of Revolution," AIAA Paper 91-3273, Sept. 1991.

[31]Visbal, M. R., "Structure of Laminar Juncture Flows," *AIAA Journal*, Vol. 29, No. 8, 1991, pp. 1273–1282.

[32]Gordnier, R. E., and Visbal, M. R., "Unsteady Vortex Structure over a Delta Wing," *Journal of Aircraft*, Vol. 31, No. 1, 1994, pp. 243–248.